

Measurement Performance Evaluation of Lateral Tire Force Sensor for Yaw-rate Control of Electric Vehicle

Daisuke Gunji^{1),2)} Hiroshi Fujimoto¹⁾

1) The University of Tokyo, Graduate School of Frontier Sciences
Transdisciplinary Sciences Bldg., 5-1-5, Kashiwanoha,
Kashiwa, Chiba, 277-8561, Japan

(E-mail: gunji@fujilab.k.u-tokyo.ac.jp, fujimoto@k.u-tokyo.ac.jp)

2) NSK Ltd.

1-5-50, Kugenumashinmei, Fujisawa, Kanagawa, 251-8501, Japan

(E-mail: gunji-d@nsk.com)

Presented at the EVTeC and APE Japan on May 22, 2014

ABSTRACT: A new advanced vehicle dynamics control is proposed in this paper for improving vehicle active safety. The lateral tire force sensor (LTFS) which directly measures lateral tire force is used for the implementation. Several performances of LTFS, the update rate, time delay, and the resolution due to the quantization and the jitter are quantified. Novel yaw-rate control method using the LTFS and yaw moment observer (YMO) is proposed and verified by simulation and experiment using experimental electric vehicle.

KEY WORDS: vehicle dynamics, motion control / lateral tire force sensor, yaw-rate control, yaw moment observer (B1)

1. Introduction

Electric vehicle has attracted attention for its environmental performances in recent years. It also has following advantages in comparison with internal combustion engine vehicles⁽¹⁾.

- From 10 to 100 times faster torque response than internal combustion engine.
- Appropriate for independent wheel drive.
- Precise torque control by motor current control.

Large numbers of studies on advanced vehicle dynamics controls have reported with aid of the advantages above⁽²⁾⁽³⁾. Our research group has proposed several yaw-rate controls for electric vehicle equipped with in-wheel motors. The cornering stiffness estimation⁽⁴⁾, and the yaw-moment observer (YMO)⁽⁵⁾ are part of the studies of our research group. These are based on the linear tire model but actual tire force characteristic has strong nonlinearity especially for large slip angle condition. Cornering stiffness also depends on road surface condition. Therefore it will not be a constant, and may suddenly change. Besides YMO requires low pass filter to suppress gyro sensor noise and the filter cause delay of yaw-rate control response. Then a sensor which directly measures tire force is required.

Lateral tire force sensor (LTFS) is under development by NSK Ltd.⁽⁶⁾. LTFS directly measures lateral tire force on the wheel hub. In this paper, we quantify the measurement performance of LTFS, the update rate, time delay, and the resolution due to the quantization and the jitter. Novel yaw-rate control method for electric

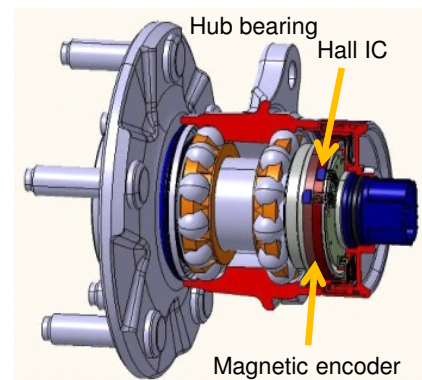


Fig. 1 Cut view of the lateral tire force sensor.

vehicle using LTFS and YMO is proposed and verified by simulation and experiment using experimental electric vehicle.

2. Experimental electric vehicle

In this research, an original experimental electric vehicle *FPEV2-Kanon* is used (shown in Fig. 2). The vehicle is developed by our research group. The vehicle has direct drive in-wheel motors (IWM) for each wheel. Uneven drive torque distribution for left and right wheels directly generates yaw moment. Front and rear axes also have electric active steering for each. Therefore the vehicle has capability of automatic steering control. LTFS which is under development in NSK Ltd. are installed in each wheel hub.

IWM of the front wheels, the front active steering, and LTFS of



Fig. 2 Experimental electric vehicle.

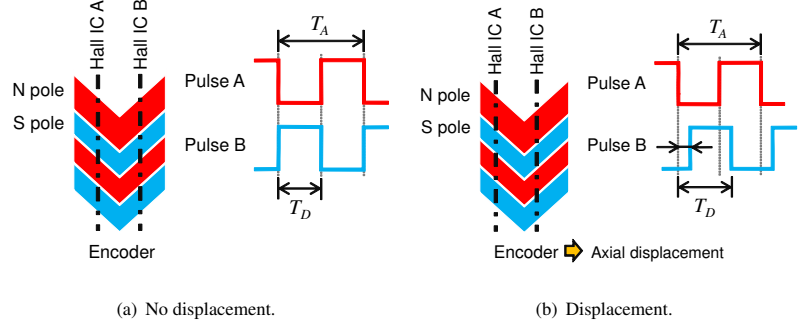


Fig. 3 Measurement principle.

Table 1 Vehicle specifications.

Vehicle Mass M	870 kg
Yaw axis inertia moment I	617 kg·m ²
Distance from CG to axle l_f, l_r	1.00, 0.70 m
Front tread base d_f	1.30 m
Tire Radius r	0.30 m
Cornering stiffness C_f, C_r	12500, 29200 N/rad
Maximum torque of front IWM	500 Nm (short time)

all wheels are involved in this research. The detailed specification of the vehicle is shown in Table 1.

3. Principle of lateral tire force sensor

LTFS is equipped on all hub unit bearing. The cross-section of the hub unit bearing including LTFS is shown in Fig. 1. The hub unit bearing consists of inner ring, outer ring, cage, and plural steel balls. Inner and outer rings axially displace due to lateral tire force. Lateral tire force is measured by calibrated correlation between lateral tire force and the axial displacement.

Principle of axial force detection is shown in Fig. 3. A magnetic encoder which has V-shape magnetic boundary is mounted on the inner ring of the hub bearing. Two magnetic Hall ICs are installed into the outer ring. Phase difference of two Hall ICs is set as to be 180 deg in electrical angle while lateral force is not applied (shown in Fig. 3(a)). The phase difference will change depending on the magnitude of lateral force, since the inner ring and the outer ring relatively displace in axial direction (shown in Fig. 3(b)). Then lateral force can be measured if the correlation between phase difference and lateral force is known.

Phase difference ratio r is defined as

$$r = \frac{T_D}{T_A}, \quad (1)$$

where T_A is pulse A period, and T_D is time difference between pulse A edge to pulse B edge. When lateral force is not acting, phase difference is 180 deg in electrical angle and $r = 0.5$.

Phase difference ratio is calculated and time-discretized on every pulse A edge timing. Then, sampling period is equal to pulse A period T_A , and it changes with vehicle velocity. Phase difference ratio at discretized time index k is calculated as

$$r_d[k] = \frac{T_{Dd}[k]}{T_{Ad}[k]}, \quad (2)$$

Table 2 Specifications of LTFS.

Encoder pulse P_n	48 pulse/rev
Base clock frequency f_{clk}	2.0 MHz
Quantization bit	16bit

where T_{Ad} and T_{Dd} are quantized time by base clock of the arithmetic processing device.

The encoder pulse signal includes periodic error due to eccentricity of the encoder surface and variability of magnetization pitch error of the encoder. In order to eliminate these errors, synchronous least mean square filter⁽⁷⁾ is applied.

Lateral force and the phase difference have nearly linear correlation. Then lateral force F_{yd} is calculated as

$$F_{yd}[k] = E r_d[k], \quad (3)$$

where E [N/-] is coefficient determined by the hub unit bearing specifications. Generally hub bearings are designed to have high rigidity to stabilize vehicle. However higher rigidity gets the sensitivity lower since the relative displacement also will be smaller. Therefore a trade-off relation exists between the rigidity and the sensitivity of LTFS. The rigidity of the LTFS should be carefully chosen to achieve both.

4. Measurement performance quantification

In this section, measurement performance of LTFS are formulated and quantified. Specifications of the LTFS which are equipped on our experimental electric vehicle are shown in Table 2.

4.1. Update rate

The phase difference ratio is calculated and time-discretized on every pulse A edge timing. It means update rate varies depending on vehicle velocity. The relation between vehicle velocity V and update rate T_{period} is calculated as

$$T_{period} = \frac{2\pi R}{P_n V}, \quad (4)$$

where R is tire radius, P_n is number of pulse per revolution of the encoder. The pulse period is quantized within limited bit width. Then maximum pulse time period exists. Measurable lower limit vehicle velocity is calculated as

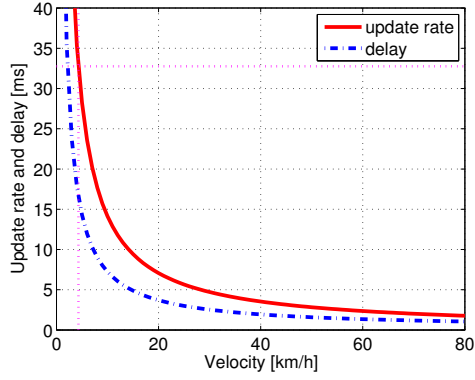


Fig. 4 Vehicle velocity v.s. update rate and delay.

$$V_{\min} = \frac{2\pi R f_{\text{clk}}}{2^m P_n}, \quad (5)$$

where f_{clk} is base clock frequency of arithmetic processing device.

In the case of our experimental vehicle, lower limit velocity is 4.3 km/h and period is 32.77 ms. Relation between v and T_{period} is shown in Fig. 4.

4.2. Time delay

The phase difference ratio at discretized time index k represents average information between pulse period $k - 1$ to k . Then the phase difference ratio $r_d[k]$ represents axial displacement at $t = t[k] - T_{Ad}[k]/2$, where $t[k]$ is time at discretized time index k . Therefore, time delay $\tau_{\text{pulse}}[k]$ is expressed as

$$\tau[k] = \tau_{\text{pulse}}[k] + \tau_{\text{proc}} = \frac{T_{Ad}[k]}{2} + \tau_{\text{proc}}, \quad (6)$$

where τ_{proc} is calculation time. In the case of our experimental vehicle, τ_{proc} is 0.17 ms by measurement. The time delay is shown in Fig. 4.

4.3. Resolution

The resolution of phase difference ratio is determined by quantization and variation in pulse edge timing.

The pulse time width is quantized by the base clock. If the pulse time width is narrower, quantized value will be smaller and the resolution will be decreasing.

When magnetic sensor IC (e.g. Hall effect IC) detects a magnetic boundary of a magnetic encoder, pulse edge variation occurs because of thermal noise⁽⁸⁾. This probabilistic phenomenon is called jitter. The frequency distribution of the jitter is known as to be close to the normal distribution. Then the frequency distribution of the phase difference ratio r_d also close to the normal distribution. In this research, the resolution by the jitter is defined as 3σ , which σ is standard deviation of the jitter.

The resolution of the phase difference ratio is shown in Fig. 5. The blue line is by quantization, and dotted red line is by the jitter. The resolution by quantization is smaller than 3×10^{-4} in 80 km/h or less. On the other hand, the resolution by the jitter is about 8×10^{-4} on every vehicle velocity. These results are obtained by using the simulated test equipment shown in Fig. 6. The

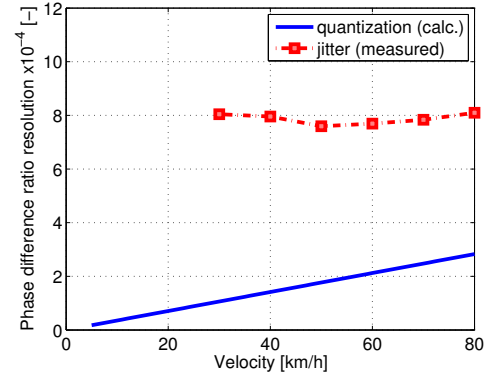


Fig. 5 Vehicle velocity v.s. resolution.

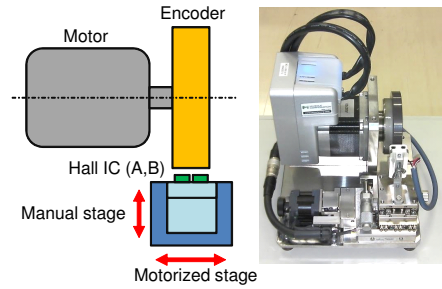


Fig. 6 Test equipment.

resolution is only determined by the jitter in this case.

5. Novel yaw-rate control method for EVs

In this section, we propose novel yaw-rate control method for EVs as application of LTFS. Our research group has proposed yaw-rate control method using yaw moment observer (YMO)⁽⁵⁾ and LTFS⁽⁹⁾. The measurement performance of LTFS was not considered in the cited literature (9), and the proposed method could not suppress direct yaw moment disturbance for example cross-wind disturbance. In this research, the effect of the measurement performance of LTFS for yaw-rate control is validated by simulation and experiment.

5.1. Vehicle model

A simple bicycle model⁽¹⁰⁾ is used for analyzing vehicle dynamics and it also used for designing control system. In the bicycle model, if vehicle velocity V is constant and body side slip angle β is small enough, vehicle dynamics are described as following motion equation

$$MV(\dot{\beta} + \gamma) = 2Y_f + 2Y_r, \quad (7)$$

$$I\dot{\gamma} = 2Y_f l_f - 2Y_r l_r + N_z, \quad (8)$$

$$Y_f \simeq -C_f \left(\beta + \frac{l_f}{V} - \delta_f \right), \quad (9)$$

$$Y_r \simeq -C_r \left(\beta - \frac{l_r}{V} \right), \quad (10)$$

where γ is yaw-rate of the vehicle, M is vehicle weight, C_f and C_r are respectively cornering stiffness of front and rear wheel, l_f and l_r are respectively distance from center of gravity to front and rear wheel axle, N_z is direct yaw moment. Cornering force Y and lateral force F_y are different, but if β is sufficiently small, they are

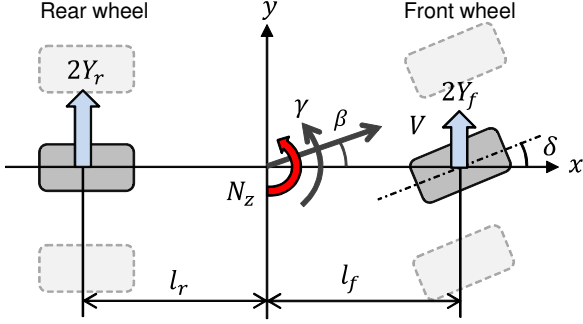


Fig. 7 Vehicle model.

regarded as same values.

Driving force is independently distributed to the left and right wheel to generate yaw moment N_z directly. Distribution law is expressed as

$$\begin{bmatrix} F_{fl} \\ F_{fr} \end{bmatrix} = \begin{bmatrix} \frac{1}{2} & -\frac{1}{d_f} \\ \frac{1}{2} & \frac{1}{d_f} \end{bmatrix} \begin{bmatrix} F_x \\ N_z \end{bmatrix}, \quad (11)$$

where F_{fl} and F_{fr} are respectively driving force of front left and front right wheel, d_f is tread width of front wheel axle, F_x is driving force command by vehicle velocity control system. Each motor torque commands are product of driving force commands and tire radius.

5.2. Yaw-rate control by YMO (conventional method)

The motion equation about yaw axis includes yaw moment disturbance N_d is expressed as following equation.

$$I\dot{\gamma} = 2Y_f l_f - 2Y_r l_r + N_d + N_z \quad (12)$$

Define N_{td} as sum of lateral force yaw moment $N_t = 2Y_f l_f - 2Y_r l_r$ and disturbance yaw moment N_d .

$$N_{td} = N_t + N_d \quad (13)$$

Then, Eq. (12) is express as

$$I\dot{\gamma} = N_{td} + N_z. \quad (14)$$

Whole N_{td} is considered as disturbance yaw moment. By composing a disturbance observer, N_{td} is compensated, and yaw motion dynamics is nominalized on bandwidth less than low-pass filter cutoff frequency ω_c in disturbance observer.

$$\gamma = \frac{1}{I_n s} N_{in} \quad (15)$$

In Eq. (15), I_n is nominal yaw axis inertia moment, N_{in} is direct yaw moment control input to the nominalized plant. This specific disturbance observer is called yaw moment observer (YMO). The block diagram of YMO is shown in Fig. 8. In order to implement disturbance observe, low-pass filter are required. The bandwidth of the feedback controller must be slower than cutoff frequency of the low-pass filter and the control performance is also limited by the low-pass filter too.

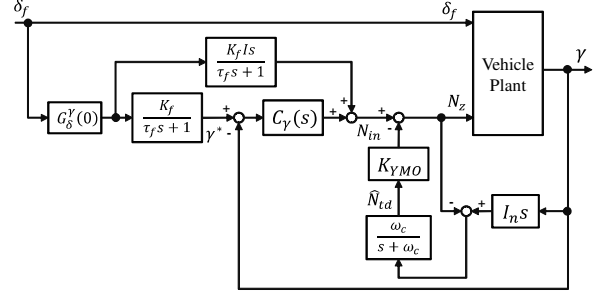


Fig. 8 Conventional method (YMO).

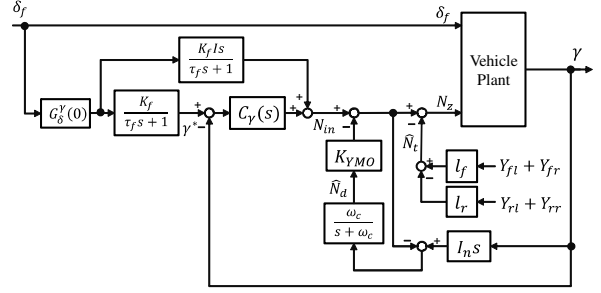


Fig. 9 Proposed method.

5.3. Yaw-rate control by LTFS and YMO (propose method)

On the normal driving condition, lateral force yaw moment N_t is dominant in yaw motion dynamics. The vehicle is supposed to be rigid in the bicycle model, but in actual certain dynamics exists from lateral tire force to vehicle yaw moment. Then yaw-rate control response performance would improve using lateral tire force measurement value by LTFS.

Lateral force yaw moment N_t is expressed as

$$N_t = (Y_{fl} + Y_{fr}) l_f - (Y_{rl} + Y_{rr}) l_r, \quad (16)$$

where Y_{ij} are measured lateral tire force by LTFS, suffix $i = f, r$ means front or rear wheel, suffix $j = l, r$ means left or right wheel.

The block diagram of the proposed control method is shown in Fig. 9. N_t is compensated on inner loop of YMO. Then equivalent plant view from YMO is expressed as follows.

$$I\dot{\gamma} = N_d + N_z \quad (17)$$

In the case of the proposed method, YMO only compensate direct disturbance yaw moment N_d . Yaw motion dynamics is nominalized same as Eq. (15). Compensation of N_t is faster than conventional method because that are directly measured. Then, yaw-rate control response performance will also be improved.

6. Simulation

The proposed and conventional methods are compared by simulations. Vehicle velocity is 30 km/h at constant, front steer angle changes sinusoidally. The amplitude is 0.05 rad and the frequency is 0.4 Hz. Without yaw-rate control, the yaw-rate by front steer is calculated as

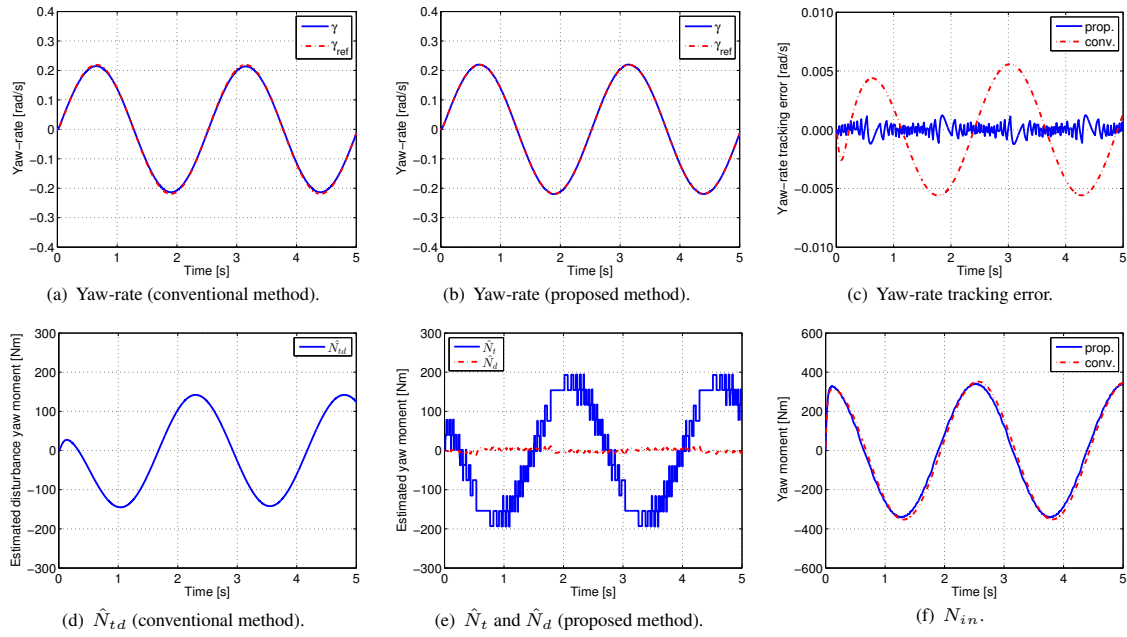


Fig. 10 Yaw-rate control simulation results.

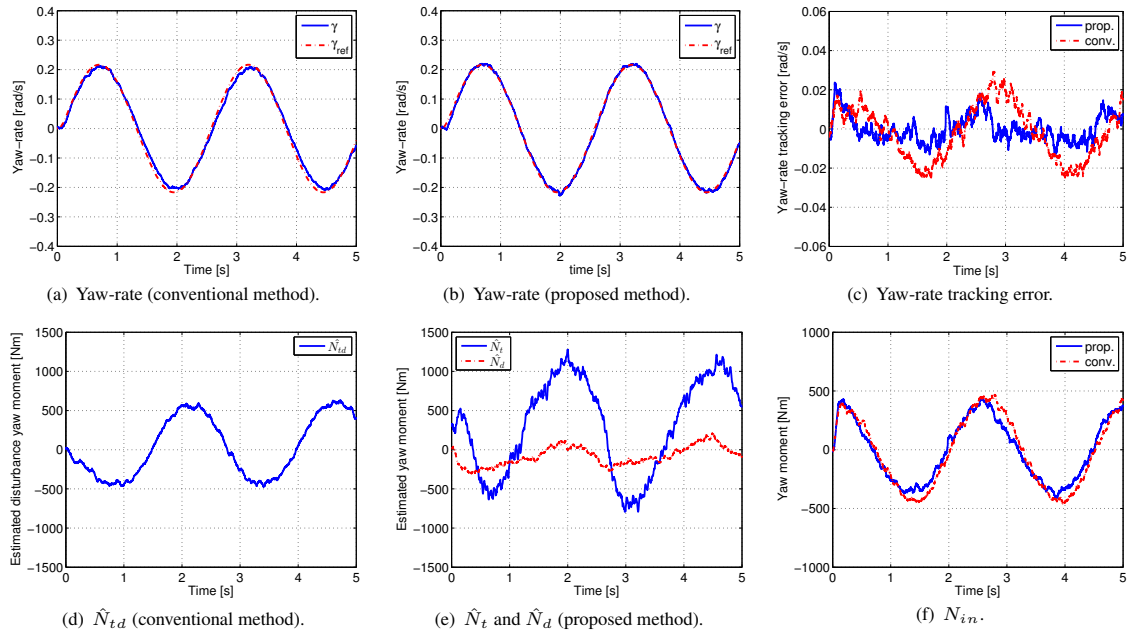


Fig. 11 Yaw-rate control experiment results.

$$G_{\delta_f}^\gamma(0) = \frac{1}{1 + AV^2} \frac{V}{l}, \quad (18)$$

where A is stability factor

$$A = -\frac{M}{2l^2} \frac{l_f C_f - l_r C_r}{C_f C_r}, \quad (19)$$

and $l = l_f + l_r$ is wheel base length⁽¹⁰⁾. In this research, reference yaw-rate is set to 1.1 times of $G_{\delta_f}^\gamma(0)$. Low-pass filter which cut-off frequency is 40 rad/s is applied to reference yaw-rate. Vehicle parameters are shown in Table 1.

The feedback controller of the yaw-rate control is a proportional controller. The controller gain is designed by pole placement

method for nominalized plant which is expressed in Eq. (15). The closed loop pole is set to -10 rad/s. The cutoff frequency of the low-pass filter on YMO is set to 10 rad/s and YMO gain K_{YMO} is set to 1.0.

The output of LTFS is calculated by using lateral force based on the bicycle model in the simulation. The lateral force is quantized and delayed based on Eq. (6), and be sampled and hold on every pulse time period based on Eq. (4). The measurement noise due to the jitter is not considered in the simulation.

The simulation results are shown in Fig. 10. Fig. 10(a) and (b) are respectively the yaw-rate response of the conventional and the

proposed method, and Fig. 10(c) is yaw-rate tracking error. In the case of the conventional method, sinusoidal tracking error occurs due to response delay of the control. On the other hand, in the case of the proposed method, the yaw-rate tracking error is well compensated in comparison with the conventional method.

Fig. 10(d) and (e) are respectively the estimated disturbance yaw moment of the conventional and the proposed method. By using the proposed method, the lateral force yaw moment and the disturbance yaw moment are independently estimated by using LTFS. Measured lateral force yaw moment is quantized due to measurement resolution of LTFS.

Fig. 10(f) is control input yaw moment N_{in} to nominalized yaw motion dynamics plant. In comparison with conventional method, N_{in} phase of proposed method close to ideal value.

In the case of conventional method, the lateral force yaw moment is estimated by YMO. Then, there is time delay due to the low-pass filter in YMO. For example, the phase of the estimated value is delayed 14.1 deg for 0.4 Hz input. That causes yaw-rate tracking error. On the other hand, in the case of the proposed method, the lateral force yaw moment is directly measured and delay is only 0.18 deg (2.53 ms) for 0.4 Hz input according to Eq. (6). Then yaw-rate tracking performance is improved by using proposed method.

7. Experiment

Vehicle experiments are conducted under the same condition as the simulation using the experimental electric vehicle. Vehicle velocity is automatically controlled to 30 km/h by velocity feedback controller. Velocity feedback controller is conducted as PI controller. Vehicle velocity is measured from rear wheel angular velocity. Front steer angle is controlled by a steer angle controller. A low-pass filter which has cutoff frequency at 20 rad/s is applied for yaw rate measurement by a gyro sensor in order to suppress the sensor noise. The same low-pass filter is also applied for lateral force measurement by LTFS in order to suppress the jitter.

The experimental results are shown in Fig. 11. Fig. 11(a) and (b) are respectively yaw-rate response of the conventional and the proposed method, and (c) is the yaw-rate tracking error. As a result of experiment, the yaw-rate tracking performance is improved by using the proposed method same as corresponding simulations.

Fig. 11(d) and (e) are respectively disturbance yaw moment of the conventional and the proposed method. Fig. 11(e) shows that almost all yaw moment is the lateral force yaw moment in this driving condition and that is measured by LTFS. Fig. 11(f) is control input yaw moment N_{in} to nominalized yaw motion dynamics plant. Phase delay is improved by using the proposed method same as corresponding simulations. Then, advantage of the proposed method is verified.

8. Conclusion

In this research, several measurement performances of LTFS are formulated and quantified. As an application of LTFS for vehicle motion control, novel yaw-rate control method is proposed. Advantage of proposed method is verified by the simulation and the

experiment, and the effect for the yaw-rate control performance due to LTFS measurement performance is discussed.

The future works are following; improving resolution of LTFS, applying the state estimation method for the better performance. The dynamics of the sprung and the unsprung masses will also be considered for improving vehicle dynamics control in addition.

Acknowledgment

This research was partly supported by Industrial Technology Research Grant Program from New Energy and Industrial Technology Development Organization(NEDO) of Japan (number 05A48701d), and by the Ministry of Education, Culture, Sports, Science and Technology grant (number 22246057).

References

- (1) Y. Hori: "Future Vehicle Driven by Electricity and Control—Research on Four-Wheel-Motored "UOT Electric March II"", IEEE Trans. Industrial Electronics, Vol.51, No.5, pp.954-962, 2004
- (2) S. Murata: "Vehicle Dynamics Innovation with In-Wheel Motor", Proc. JSAE EVTeC'11, 20117204, Yokohama, 2011
- (3) S. J. Hallowell, and L. R. Ray: "All-Wheel Driving Using Independent Torque Control of Each Wheel", Proc. American Control Conference, Vol.3, pp.2590-2595, Denver, 2003
- (4) N. Takahashi, and H. Fujimoto: "Consideration on Yaw Rate Control for Electric Vehicle Based on Cornering Stiffness and Body Slip Angle Estimation", Proc. IEEJ IIC-06-04, pp.17-22, 2006 (in Japanese)
- (5) H. Fujimoto, T.Saito, T. Noguchi: "Motion Stabilization Control of Electric Vehicle under Snowy Conditions Base on Yaw-Moment Observer", IEEE Int. workshop advanced motion control, pp.35-40, 2004
- (6) K. Ono, T. Takizawa, and M. Aoki: "Preload measuring device for double row rolling bearing unit" U.S. Patent 20090052825A1, 2009
- (7) H. Hamada, K. Ito, and S. Uto: "Synchronised Filtered-x Algorithm and its Application to Active Noise Control", Proc. JSME Environmental engineering synthesis symposium, pp.46-50, 1992 (in Japanese)
- (8) M. Motz, D.Draxelmayr, T. Werth, and B. Forster: "A Chopped Hall Sensor With Small Jitter and Programmable "True Power-On" Function", IEEE Journal of Solid-state circuits, Vol.40, No.7, pp.1533-1540, 2005
- (9) Y. Yamauchi, and H. Fujimoto: "Yaw-rate Control Method of Electric Vehicle with Tire Lateral Force Sensor", Proc. IEEJ IIC-09-24, pp.19-24, 2009 (in Japanese)
- (10) M. Abe: "Automotive Vehicle Dynamics Theory and Applications", Tokyo Denki Univ. publishing, 2008 (in Japanese)